

# A nonideal error-field response model for strongly shaped tokamak plasmas

R. Fitzpatrick

Department of Physics, Institute for Fusion Studies, University of Texas at Austin,  
Austin, Texas 78712, USA

(Received 17 September 2010; accepted 30 September 2010; published online 4 November 2010)

A model is developed that describes the error-field response of a toroidally rotating tokamak plasma possessing a strongly shaped poloidal cross-section. The response is made up of nondissipative ideal and dissipative nonideal components. The calculation of the ideal response is greatly simplified by employing a large aspect-ratio, constant pressure plasma equilibrium in which the current is entirely concentrated at the boundary. Moreover, the calculation of the resonant component of the nonideal response is simplified by modeling each resonant surface within the plasma as a toroidally rotating, thin resistive shell that only responds to the appropriate resonant component of the perturbed magnetic field. This approach mimics dissipation due to continuum damping at Alfvén and/or sound wave resonances inside the plasma. The nonresonant component of the nonideal response is neglected. The error-fields that maximize the net toroidal locking torque exerted on the plasma are determined via singular value decomposition of the total response matrix. For a strongly dissipative plasma, the locking torque associated with a general error-field is found to peak at a beta value that lies *above* the no-wall beta-limit, in accordance with experimental observations. © 2010 American Institute of Physics. [doi:10.1063/1.3504227]

## I. INTRODUCTION

Tokamak<sup>1</sup> plasmas are highly sensitive to externally generated, static magnetic perturbations that break axisymmetry.<sup>2–6</sup> Such perturbations, which are conventionally termed *error-fields*, are present in all tokamak experiments because of imperfections in magnetic field-coils. An error-field can drive *magnetic reconnection* in an otherwise tearing stable plasma, giving rise to the formation of *locked* (i.e., nonrotating) *magnetic island chains* at internal resonant magnetic flux-surfaces.<sup>7</sup> Such chains severely degrade global energy confinement.<sup>8</sup> Fortunately, the (highly sub-Alfvénic) toroidal rotation that occurs naturally in all tokamak plasmas affords them some level of protection against locked mode formation. To be more exact, rotation induces localized *shielding currents* at the various resonant surfaces within the plasma, and these currents *suppress* driven reconnection. Provided that this suppression is sufficiently strong, it is an excellent first approximation to say that the response of a rotating tokamak plasma to a low amplitude error-field is governed by *linearized marginally stable ideal-magnetohydrodynamics* (MHD).<sup>9</sup> Unfortunately, the residual magnetic reconnection at the resonant surfaces, which is associated with plasma *dissipation*, produces a toroidal *locking torque* that slows the plasma rotation. Moreover, the rotation is suddenly arrested when the error-field amplitude exceeds a certain critical value, which permits locked mode formation to proceed without further hindrance.<sup>10,11</sup> This scenario is generally referred to as *error-field penetration*. The critical error-field amplitude required to trigger penetration can be as small as  $10^{-4}$  of the equilibrium toroidal field-strength.

This paper investigates the relationship between the *harmonic content* of an error-field and the associated locking torque that is exerted on the plasma. Such an investigation is

crucial to the determination of which error-field harmonics need to be cancelled out by error-field correction coils in order to prevent locked mode formation. Of course, the relationship in question is very simple in a quasicylindrical tokamak (i.e., a large aspect-ratio, low-beta, tokamak with a circular poloidal cross-section). As is well-known, there is no coupling between different poloidal and toroidal harmonics in a cylindrically symmetric plasma equilibrium. Consequently, an  $m, n$  error-field—where  $m$  is the poloidal mode number and  $n$  the toroidal mode number—only exerts a torque at the  $m, n$  resonant surface—which is defined as the magnetic flux-surface that satisfies the resonance condition  $q=m/n$ , where  $q$  is the safety-factor (i.e., the inverse of the rotational transform). Conversely, if no such surface lies within the plasma then no torque is generated. It follows that the only harmonics of an error-field which need to be cancelled out in a quasicylindrical tokamak are those which are resonant within the plasma. Unfortunately, real tokamak plasmas are not quasicylindrical—mainly, because they possess magnetic flux-surfaces with highly *elongated* and *triangular* poloidal cross-sections. The consequent deviations from cylindrical symmetry give rise to *coupling* between poloidal harmonics with different mode numbers.<sup>12</sup> Under these circumstances, recent numerical calculations have demonstrated that the relationship between the harmonic content of an error-field and the locking torque can be *substantially different* to that in a quasicylindrical tokamak.<sup>13–15</sup> The first goal of this paper is to construct a simplified (relative to the aforementioned numerical calculations) model of the former relationship that is as realistic as possible. The second goal is to incorporate the nonideal response of the plasma (see below) into the model in a self-consistent manner (this was not attempted in Refs. 13–15).

The response of a tokamak plasma to an error-field can be divided into ideal and nonideal components. The *ideal response* consists of perturbed currents produced by the error-field induced *distortion* of the equilibrium magnetic flux-surfaces, in combination with the localized shielding currents that suppress driven magnetic reconnection at the internal resonant surfaces. As the name suggests, the ideal response of the plasma is that predicted by linearized marginally stable ideal-MHD.<sup>9</sup> The main difference between the error-field response of a quasicylindrical and a highly shaped tokamak is that, in the former case, the ideal response is dominated by the shielding currents, whereas, in the latter case, the shielding currents only form a relatively small part of the overall ideal response.<sup>13–15</sup>

The *nonideal response* of the plasma cannot be described by ideal-MHD. The resonant component of this response is associated with dissipation (and residual reconnection) at the plasma's internal resonant surfaces. Moreover, it is the resonant nonideal response which is responsible for the locking torque acting on the plasma. The *nonresonant* component of the nonideal response is associated with *nonambipolar particle transport* induced by the applied error-field's lack of axisymmetry<sup>16</sup> and gives rise to an electromagnetic braking torque acting on the plasma. However, such a torque cannot directly trigger error-field penetration (since it does not have the correct type of nonmonotonic variation with the plasma rotation).<sup>17</sup> Hence, in this paper, we shall only consider the resonant component of the nonideal plasma response.

The calculation of the ideal plasma response can be greatly simplified by adopting a *large aspect-ratio* equilibrium in which the pressure is *uniform*, and the current entirely concentrated at the boundary.<sup>18</sup> This approach allows us to replace the volume distributed perturbed currents which constitute the plasma's ideal response by equivalent surface currents flowing on the plasma boundary. As is well-known, it is possible to allow for significant *vertical elongation* of a constant pressure equilibrium in a relatively straightforward manner by solving Poisson's equation (for the perturbed magnetic potential) in orthogonal elliptic coordinates.<sup>19</sup> Unfortunately, this method of solution cannot be directly generalized to allow for significant plasma *triangularity* because, in the presence of triangularity, it is impossible to find an orthogonal coordinate system that is nonsingular both inside and outside the plasma. One alternative is to employ Green's function technique to solve Poisson's equation.<sup>20</sup> However, this solution method is highly inconvenient since it entails the evaluation of singular integrals. In this paper, a much more convenient solution method is developed which uses separate nonorthogonal and orthogonal curvilinear coordinate systems inside and outside the plasma, respectively.

Finally, the calculation of the resonant nonideal response of the plasma can be simplified by modeling each internal resonant surface as a *toroidally rotating, thin resistive shell* that only responds to the appropriate resonant harmonic of the perturbed magnetic field. In a further simplification, it is assumed that the shells are all located at the plasma boundary. This approach allows us to replace the internal perturbed currents which make up the plasma's resonant nonideal response by equivalent surface currents flowing on the plasma

boundary. In addition, the approach mimics dissipation due to *continuum damping* at closely separated *Alfvén resonances* straddling the resonant flux-surfaces of a toroidally rotating (at a highly sub-Alfvénic velocity) tokamak plasma interacting with a static magnetic perturbation.<sup>21–23</sup> More realistically, the approach also mimics continuum damping at *sound wave resonances* located close to each resonant surface.<sup>24,25</sup>

## II. PLASMA EQUILIBRIUM

### A. Normalization

All lengths are normalized to the horizontal semi-axis of the plasma,  $a$ , and all magnetic field-strengths to the on-axis vacuum toroidal field-strength,  $B_0$ .

### B. Large aspect-ratio ordering

The *inverse aspect-ratio* of the plasma is defined as

$$\epsilon \equiv \frac{a}{R_0}, \quad (1)$$

where  $R_0$  is the major radius at the magnetic axis. In the following, the conventional *large aspect-ratio* ordering,

$$0 < \epsilon \ll 1, \quad (2)$$

is adopted.

### C. Coordinate systems

Let  $x, y, z$  be a right-handed Cartesian coordinate system such that  $x, y$ , and  $z$  are, respectively, horizontal and vertical coordinates in the poloidal plane, and a pseudotoroidal coordinate that is periodic with period  $2\pi/\epsilon$ . The effective magnetic axis of the plasma lies at  $x=y=0$ .

Let  $r, \theta, \phi$  be a right-handed, axisymmetric, curvilinear coordinate system which is such that  $r(x, y)$ ,  $\theta(x, y)$ , and  $\phi \equiv \epsilon z$  are, respectively, a radial coordinate (in the poloidal plane), a poloidal angle, and a pseudotoroidal angle. The magnetic axis lies at  $r=0$ , and the outboard midplane of the plasma corresponds to  $\theta=0$ . Let  $\mathbf{e}_r \equiv \nabla r / |\nabla r|$ ,  $\mathbf{e}_\theta \equiv \nabla \theta / |\nabla \theta|$ , and  $\mathbf{e}_\phi \equiv \nabla \phi / |\nabla \phi|$ .

### D. Plasma boundary

The plasma boundary corresponds to the axisymmetric toroidal surface  $r=1$ . Let the parametric equation of the boundary in the poloidal plane,  $x=x_p(\theta)$ ,  $y=y_p(\theta)$ , take the form

$$x_p(\theta) = \cos \theta + \delta \cos 2\theta, \quad (3)$$

$$y_p(\theta) = \kappa \sin \theta - \delta \sin 2\theta, \quad (4)$$

where  $\kappa \geq 0$  is the plasma vertical elongation and  $\delta \geq 0$  the plasma triangularity.

### E. Pressure balance

The plasma equilibrium used in this paper is such that the internal pressure is uniform, and the current entirely concentrated on the *boundary*.<sup>18–20</sup> Thus, the internal magnetic field can be written as

$$\mathbf{B}(r < 1, \theta) = \frac{1 - \epsilon b_i}{1 + \epsilon x(r, \theta)} \mathbf{e}_\phi, \quad (5)$$

where  $b_i \sim \mathcal{O}(1)$  is a positive constant. Note that there is no internal poloidal field. The external magnetic field takes the form

$$\mathbf{B}(r > 1, \theta) = \epsilon B_r(r, \theta) \mathbf{e}_r + \epsilon B_\theta(r, \theta) \mathbf{e}_\theta + \frac{\mathbf{e}_\phi}{1 + \epsilon x(r, \theta)}, \quad (6)$$

where  $B_r, B_\theta \sim \mathcal{O}(1)$ . However,

$$B_r(1_+, \theta) = 0, \quad (7)$$

since the boundary must be a magnetic flux-surface. Let

$$B_p(\theta) \equiv B_\theta(1_+, \theta) \quad (8)$$

be the poloidal magnetic field (normalized to  $\epsilon B_0$ ) immediately outside the boundary.

The uniform internal plasma pressure (normalized to  $B_0^2/2\mu_0$ ) is written as

$$P = \epsilon \beta, \quad (9)$$

where  $\beta \sim \mathcal{O}(1)$  is a positive constant that corresponds to the conventional toroidal beta divided by  $\epsilon$ . Furthermore, pressure balance across the boundary,

$$P + B^2(1_-, \theta) = B^2(1_+, \theta), \quad (10)$$

yields<sup>18–20</sup>

$$B_p(\theta) = (2\beta[\alpha_p + x_p(\theta)])^{1/2} + \mathcal{O}(\epsilon), \quad (11)$$

where  $\alpha_p \sim \mathcal{O}(1)$  is a positive constant. Finally, the *edge safety-factor* of the plasma is defined as

$$q_p = \frac{1}{\pi} \int_0^\pi \frac{h_p}{B_p} d\theta, \quad (12)$$

where

$$\begin{aligned} h_p(\theta) &\equiv \left[ \left( \frac{dx_p}{d\theta} \right)^2 + \left( \frac{dy_p}{d\theta} \right)^2 \right]^{1/2} \\ &= (1 - E_p)^{-1} (1 + E_p^2 + 4T_p^2 - 4E_p T_p \cos \theta \\ &\quad + 2E_p \cos 2\theta - 4T_p \cos 3\theta)^{1/2}. \end{aligned} \quad (13)$$

Here,

$$E_p = \frac{\kappa - 1}{\kappa + 1}, \quad (14)$$

$$T_p = \frac{2\delta}{\kappa + 1} \quad (15)$$

are convenient measures of the plasma ellipticity and triangularity, respectively.

### III. PERTURBED PLASMA EQUILIBRIUM

#### A. Perturbed magnetic field

Consider the response of the plasma to a small amplitude, quasistatic, externally generated, nonaxisymmetric magnetic perturbation. According to linearized marginally stable ideal-MHD theory,<sup>9</sup> the perturbed internal plasma

current and pressure are both zero in a constant pressure equilibrium. Hence, the perturbed magnetic field within the plasma boundary can be written in the form

$$\delta \mathbf{B} = i \epsilon \nabla V, \quad (16)$$

where

$$\nabla^2 V(r, \theta, \phi) = 0. \quad (17)$$

Of course, the perturbed magnetic field in the vacuum region outside the boundary can also be written in this form.

#### B. External solution

In the external region,  $r > 1$ , let

$$x(r, \theta) = (1 - E_p)^{-1} \left( r \cos \theta - \frac{E_p}{r} \cos \theta + \frac{T_p}{r^2} \cos 2\theta \right), \quad (18)$$

$$y(r, \theta) = (1 - E_p)^{-1} \left( r \sin \theta + \frac{E_p}{r} \sin \theta - \frac{T_p}{r^2} \sin 2\theta \right). \quad (19)$$

It follows that  $|\nabla r| = r|\nabla \theta| = h^{-1}$  and  $\nabla r \cdot \nabla \theta = 0$ , where

$$\begin{aligned} h(r, \theta) &= (1 - E_p)^{-1} \left( 1 + \frac{E_p^2}{r^4} + \frac{4T_p^2}{r^6} - \frac{4E_p T_p}{r^5} \cos \theta \right. \\ &\quad \left. + \frac{2E_p}{r^2} \cos 2\theta - \frac{4T_p}{r^3} \cos 3\theta \right)^{1/2}. \end{aligned} \quad (20)$$

Note, from Eqs. (3), (4), and (13)–(15) that  $x(1, \theta) = x_p(\theta)$ ,  $y(1, \theta) = y_p(\theta)$ , and  $h(1, \theta) = h_p(\theta)$ . The  $r, \theta, \phi$  coordinate system is nonsingular throughout the external region as long as  $\delta < \kappa/2$ .

Let

$$V(r, \theta, \phi) = \sum_m V_m(r) e^{i(m\theta - n\phi)}, \quad (21)$$

where  $n > 0$  is the *toroidal mode number* of the external magnetic perturbation. In the limit  $n\epsilon \ll 1$ , Laplace's equation (17) yields

$$r \frac{d}{dr} \left( r \frac{dV_m}{dr} \right) - m^2 V_m = 0. \quad (22)$$

In the absence of either a conducting or a resistive wall surrounding the plasma, the general solution to the above equation is

$$V_m(r) = a_m r^{-|m|} + b_m r^{|m|} \quad (23)$$

for  $m \neq 0$ , and

$$V_0(r) = a_0 \ln r + b_0, \quad (24)$$

where the  $a_m$  and  $b_m$  are constants. It follows that

$$V_m(1_+) = -|m|^{-1} r \left. \frac{dV_m}{dr} \right|_{1_+} + 2b_m \quad (25)$$

for  $m \neq 0$ ,

$$V_0(1_+) = b_0 \quad (26)$$

and

$$r \left. \frac{dV_0}{dr} \right|_{1+} = a_0. \quad (27)$$

The externally generated component of the perturbed field is written as

$$\delta \mathbf{B}_e = i \epsilon \nabla V_e, \quad (28)$$

where

$$V_e(r, \theta, \phi) = \sum_m b_m r^{|m|} e^{i(m\theta - n\phi)}. \quad (29)$$

Let

$$\Phi(\theta, \phi) = \left. \frac{\mathbf{e}_r \cdot \delta \mathbf{B}_e}{|\nabla \theta| |\nabla \phi|} \right|_{r=1} \quad (30)$$

be the normal flux per unit solid angle (normalized to  $B_0 a^2$ ) of the *externally generated* nonaxisymmetric field at the plasma boundary. It follows that

$$\Phi(\theta, \phi) = i \sum_{m \neq 0} \Phi_m e^{i(m\theta - n\phi)}, \quad (31)$$

where

$$\Phi_m = |m| b_m. \quad (32)$$

Let

$$\chi(\theta, \phi) = \left. \frac{\mathbf{e}_r \cdot \delta \mathbf{B}}{|\nabla \theta| |\nabla \phi|} \right|_{r=1+} \quad (33)$$

be the normal flux per unit solid angle (normalized to  $B_0 a^2$ ) of the *total* nonaxisymmetric field (i.e., the sum of the externally generated and plasma generated fields) just outside the plasma boundary. It follows that

$$\chi(\theta, \phi) = i \sum_{m \neq 0} \chi_m e^{i(m\theta - n\phi)}, \quad (34)$$

where

$$\chi_m = |m| (b_m - a_m) = r \left. \frac{dV_m}{dr} \right|_{1+}. \quad (35)$$

### C. Ideal plasma response

In the internal region,  $0 < r < 1$ , let

$$x(r, \theta) = (1 - E_p)^{-1} [r \cos \theta - E(r) \cos \theta + T(r) \cos 2\theta], \quad (36)$$

$$y(r, \theta) = (1 - E_p)^{-1} [r \sin \theta + E(r) \sin \theta - T(r) \sin 2\theta], \quad (37)$$

where

$$E(r) = \begin{cases} 0 & 0 \leq r \leq r_0 \\ [(r - r_0)/(r_1 - r_0)](E_p/r_1) & r_0 < r < r_1 \\ E_p/r & r_1 \leq r \leq 1, \end{cases} \quad (38)$$

$$T(r) = \begin{cases} 0 & 0 \leq r \leq r_0 \\ r[(r - r_0)/(r_1 - r_0)](T_p/r_1^3) & r_0 < r < r_1 \\ T_p/r^2 & r_1 \leq r \leq 1, \end{cases} \quad (39)$$

and  $0 < r_0 < r_1 < 1$ . It follows, from Eqs. (3), (4), (14), and (15) that  $x(1, \theta) = x_p(\theta)$  and  $y(1, \theta) = y_p(\theta)$ . Note that the internal  $r, \theta, \phi$  coordinate system coincides with external system (18) and (19) in the region  $r_1 \leq r \leq 1$ . In the limit  $r_0 \rightarrow 0$  and  $r_1 \rightarrow 1$ , the  $r, \theta, \phi$  coordinate system is nonsingular throughout the internal region as long as  $\delta < 1/2$ .

Now, it is easily demonstrated that

$$(\nabla r \times \nabla \theta \cdot \nabla z)^{-1} = (1 - E_p)^{-2} r \mathbf{J}, \quad (40)$$

$$|\nabla r|^2 = \frac{a_{rr}}{J^2}, \quad (41)$$

$$\nabla r \cdot \nabla \theta = \frac{a_{r\theta}}{r^2 J^2}, \quad (42)$$

$$|\nabla \theta|^2 = \frac{a_{\theta\theta}}{r^2 J^2}, \quad (43)$$

where

$$\begin{aligned} J = 1 - \frac{EE'}{r} - \frac{2TT'}{r} + \left( \frac{ET'}{r} + \frac{2E'T}{r} \right) \cos \theta \\ + \left( \frac{E}{r} - E' \right) \cos 2\theta - \left( \frac{2T}{r} - T' \right) \cos 3\theta, \end{aligned} \quad (44)$$

$$a_{rr} = 1 + \frac{E^2}{r^2} + \frac{4T^2}{r^2} - \frac{4ET}{r^2} \cos \theta + \frac{2E}{r} \cos 2\theta - \frac{4T}{r} \cos 3\theta, \quad (45)$$

$$\begin{aligned} a_{r\theta} = \left( \frac{2E'T}{r} - \frac{ET'}{r} \right) \sin \theta - \left( \frac{E}{r} + E' \right) \sin 2\theta \\ + \left( \frac{2T}{r} + T' \right) \sin 3\theta, \end{aligned} \quad (46)$$

$$\begin{aligned} a_{\theta\theta} = 1 + E'^2 + T'^2 - 2E'T' \cos \theta - 2E' \cos 2\theta \\ + 2T' \cos 3\theta. \end{aligned} \quad (47)$$

Here,  $' \equiv d/dr$ .

In the limit  $n\epsilon \ll 1$ , Laplace's equation (17) yields

$$r \frac{dV_m}{dr} = \sum_{m'} (Q_{mm'} \psi_{m'} - R_{mm'} V_{m'}), \quad (48)$$

$$r \frac{d\psi_m}{dr} = \sum_{m'} (R_{m'm} \psi_{m'} - S_{mm'} V_{m'}), \quad (49)$$

where

$$\psi_m(r) = \sum_{m'} \left( \mathcal{L}_{mm'} r \frac{dV_{m'}}{dr} + \mathcal{M}_{mm'} V_{m'} \right) \quad (50)$$

and

$$Q_{mm'}(r) = (\mathcal{L}^{-1})_{mm'}, \quad (51)$$

$$R_{mm'}(r) = \sum_k (\mathcal{L}^{-1})_{mk} \mathcal{M}_{km'}, \quad (52)$$

$$S_{mm'}(r) = \sum_k \mathcal{M}_{km} R_{km'} + \mathcal{P}_{mm'}, \quad (53)$$

with

$$\mathcal{L}_{mm'}(r) = \frac{1}{\pi} \int_0^\pi \frac{a_{rr}}{J} \cos[(m-m')\theta] d\theta, \quad (54)$$

$$\mathcal{M}_{mm'}(r) = \frac{m'}{\pi} \int_0^\pi \frac{a_{r\theta}}{J} \sin[(m-m')\theta] d\theta, \quad (55)$$

$$\mathcal{P}_{mm'}(r) = -\frac{mm'}{\pi} \int_0^\pi \frac{a_{\theta\theta}}{J} \cos[(m-m')\theta] d\theta. \quad (56)$$

Note that  $Q_{m'm} = Q_{mm'}$  and  $S_{m'm} = S_{mm'}$ . Furthermore, Eqs. (48) and (49) can be combined to give

$$r \frac{d}{dr} \left( \sum_m V_m \psi_m \right) = \sum_{m,m'} (Q_{mm'} \psi_m \psi_{m'} - S_{mm'} V_m V_{m'}). \quad (57)$$

Observe that  $E(r)$  and  $T(r)$  are continuous in the internal region, whereas  $E'(r)$  and  $T'(r)$  are discontinuous at  $r=r_0$  and  $r=r_1$ . It follows that the  $Q_{mm'}$ ,  $R_{mm'}$ , and  $S_{mm'}$  functions are also discontinuous at  $r=r_0$  and  $r=r_1$ . Despite this, as is clear from Eqs. (48) and (49), the  $V_m(r)$  and  $\psi_m(r)$  functions are continuous throughout the internal region.

The *ideal* (i.e., linearized marginally stable ideal-MHD) response of the plasma to the external perturbation is determined by launching a series of well-behaved (at  $r=0$ ) solutions of Eqs. (48) and (49) from  $r=r_0$ , and then integrating them to  $r=r_1$ . (Incidentally, launching the solutions from  $r=r_0$ , where  $r_0 > 0$ , rather than from  $r=0$ , alleviates numerical problems associated with the rapid growth of  $r^{|m|}$  solutions, at small- $r$ , when  $|m| \gg 1$ .) In the region  $0 \leq r \leq r_0$ , it is easily demonstrated that  $Q_{mm'} = \delta_{mm'}$ ,  $R_{mm'} = 0$ , and  $S_{mm'} = -m^2 \delta_{mm'}$ . Equations (48) and (49) consequently reduce to Eq. (22). Hence, at  $r=r_0$ , the  $m$ th well-behaved solution is written as

$$V_{m'}(r_0) = r_0^{|m|} \delta_{mm'}, \quad (58)$$

$$\psi_{m'}(r_0) = |m| r_0^{|m|} \delta_{mm'}. \quad (59)$$

Let

$$A_{mm'} = V_{m'}(r_1), \quad (60)$$

$$B_{mm'} = \psi_{m'}(r_1). \quad (61)$$

Now, it is easily demonstrated that the  $m=0$  solution takes the particularly simple form

$$V_{m'}(r) = \delta_{0m'}, \quad (62)$$

$$\psi_{m'}(r) = 0, \quad (63)$$

throughout the internal region. It follows that

$$A_{0m'} = \delta_{0m'}, \quad (64)$$

$$B_{0m'} = 0. \quad (65)$$

It is also readily shown that  $\psi_0(r)=0$  in region  $0 < r < 1$  for all solutions, which implies that

$$B_{m0} = 0. \quad (66)$$

Finally, the  $C_{mm'}$  values are determined from

$$A_{mm'} = \sum_k B_{mk} C_{km'} + \delta_{0m} \delta_{0m'}. \quad (67)$$

Note that the  $C_{m0}$  are arbitrary, since the  $B_{m0}$  are all zero.

In the region  $r_1 \leq r \leq 1$ , it is easily demonstrated that  $Q_{mm'} = \delta_{mm'}$ ,  $R_{mm'} = 0$ ,  $S_{mm'} = -m^2 \delta_{mm'}$ , and consequently that  $\psi_m = r dV_m/dr$ . It is convenient to take the limit  $r_1 \rightarrow 1_-$ , in which case

$$V_m(1_-) = V_m(r_1), \quad (68)$$

$$r \left. \frac{dV_m}{dr} \right|_{1_-} = \psi_m(r_1). \quad (69)$$

It follows, from the above analysis, that the ideal response of the plasma to the external perturbation is specified by

$$V_m(1_-) = \sum_{m'} C_{mm'} r \left. \frac{dV_{m'}}{dr} \right|_{1_-} \quad (70)$$

for  $m \neq 0$  and

$$V_0(1_-) = \sum_{m'} C_{0m'} r \left. \frac{dV_{m'}}{dr} \right|_{1_-} + c_0, \quad (71)$$

where  $c_0$  is a constant. Furthermore, the fact that the  $B_{m0}$  are all zero implies that

$$\psi_0(1_-) = r \left. \frac{dV_0}{dr} \right|_{1_-} = 0. \quad (72)$$

Now, integrating Eq. (57) from  $r=0$  to  $r=1_-$ , making use of the boundary conditions at  $r=0$ , as well as Eqs. (70) and (72), we obtain

$$\begin{aligned} & \sum_{m,m' \neq 0} C_{mm'} \psi_m(1_-) \psi_{m'}(1_-) \\ &= \sum_{mm'} \int_0^1 (Q_{mm'} \psi_m \psi_{m'} - S_{mm'} V_m V_{m'}) dr. \end{aligned} \quad (73)$$

Swapping the indices  $m$  and  $m'$  taking the difference between the resulting two equations, and recalling that  $Q_{m'm} = Q_{mm'}$  and  $S_{m'm} = S_{mm'}$ , we deduce that

$$\sum_{m,m' \neq 0} (C_{mm'} - C_{m'm}) \psi_m(1_-) \psi_{m'}(1_-) = 0. \quad (74)$$

Since the above equation is true for arbitrary  $\psi_m(1_-)$ , it follows that  $C_{m'm} = C_{mm'}$  for all  $m, m' \neq 0$ . Moreover, given that the  $C_{m0}$  are arbitrary, we can set  $C_{m0} = C_{0m}$  for  $m \neq 0$  and  $C_{00} = 0$ . Hence, we conclude that

$$C_{m'm} = C_{mm'} \quad (75)$$

for all  $m$  and  $m'$ . The above symmetry relation is ultimately a consequence of the well-known self-adjointness of the ideal-MHD force operator.<sup>9</sup> It also ensures that the plasma cannot exert a toroidal torque on itself.<sup>12</sup>

#### D. Nonideal plasma response

We can simulate the *resonant nonideal* response of the plasma, which is associated with dissipation at internal resonant surfaces, by modeling each such surface as a toroidally rotating, thin resistive shell that only responds to the appropriate resonant harmonic of the perturbed magnetic field.

Let  $\delta \mathbf{j}(\theta, \phi)$  be the current density (normalized to  $\epsilon B_o / a \mu_0$ ) in a particular resistive shell lying on the axisymmetric toroidal surface  $r = r_s$ . Integrating

$$\nabla \times \delta \mathbf{B} = \delta \mathbf{j} \quad (76)$$

(in  $r$ ) across the shell, we obtain

$$\mathbf{J}(\theta, \phi) = \mathbf{ie}_r \times \nabla \mathcal{J}, \quad (77)$$

where

$$\mathbf{J}(\theta, \phi) = \int_{r_{s-}}^{r_{s+}} \delta \mathbf{j} \frac{dr}{|\nabla r|} \quad (78)$$

is the radially integrated current density in the shell (normalized to  $\epsilon B_o / \mu_0$ ), and

$$\mathcal{J}(\theta, \phi) = [V]_{r=r_{s-}}^{r=r_{s+}} \quad (79)$$

is a current stream-function (normalized to  $\epsilon B_o / \mu_0$ ). Note that  $r_{s\pm} = r_s \pm \delta_s/2$ , where  $\delta_s \ll 1$  is the constant shell thickness (in  $r$ ). Now, integration of

$$\nabla \cdot \delta \mathbf{B} = 0 \quad (80)$$

(in  $r$ ) across the shell yields

$$\left[ r \frac{\partial V}{\partial r} \right]_{r=r_{s-}}^{r=r_{s+}} = 0. \quad (81)$$

Finally, the radial component of the curl of Ohm's law within the shell gives

$$in\Omega'_s \delta B_r = \mathbf{e}_r \cdot \nabla \times (\sigma_s^{-1} \delta \mathbf{j}), \quad (82)$$

where  $\Omega'_s = \Omega_s - \omega/n$ ,  $\Omega_s$  is the shell toroidal angular velocity,  $\omega$  the real frequency of both the applied perturbation and the plasma response (this frequency assumed to be much less than the Alfvén frequency, so that the perturbed plasma is effectively in a nonaxisymmetric equilibrium state), and  $\sigma_s(\theta)$  the shell electrical conductivity. It follows that

$$in\Omega'_s r \left. \frac{\partial V}{\partial r} \right|_{r=r_s} = \frac{\partial}{\partial \theta} \left( \tau_s^{-1} \frac{\partial \mathcal{J}}{\partial \theta} \right), \quad (83)$$

where

$$\tau_s(\theta) = r_s \delta_s h_s^2 \sigma_s \quad (84)$$

is the shell time-constant, and

$$h_s(\theta) \equiv h(r_s, \theta). \quad (85)$$

Consider the simulated  $m, n$  resonant surface. By analogy with Eqs. (11) and (12), the poloidal magnetic field at this surface is modeled as

$$B_m(\theta) = (2\beta[\alpha_m + x_p(\theta)])^{1/2}, \quad (86)$$

where the constant  $\alpha_m$  is adjusted so as to ensure that

$$\frac{1}{\pi} \int_0^\pi \frac{h_m}{B_m} d\theta = q_m. \quad (87)$$

Here,

$$h_m(\theta) \equiv h(r_m, \theta), \quad (88)$$

where  $r_m$  is the shell radius and

$$q_m = \frac{m}{n}. \quad (89)$$

Let us define the “straight” poloidal angle,

$$\nu_m(\theta) = \int_0^\theta \rho_m(\theta') d\theta', \quad (90)$$

where

$$\rho_m(\theta) = \frac{h_m}{q_m B_m}. \quad (91)$$

Thus, in the  $\nu_m - \phi$  plane, the equilibrium magnetic field-lines at the resonant surface take the form of *straight-lines* of constant gradient  $d\nu_m/d\phi = 1/q_m$ . Let

$$[V]_{r=r_{m-}}^{r=r_{m+}} = \mathcal{J}(\theta, \phi) = \sum_{m'} \mathcal{J}_{m'} e^{i[m' \nu_m(\theta) - n\phi]}, \quad (92)$$

where the  $\mathcal{J}_m$  are constants. Furthermore, by analogy with Eq. (83), let us write

$$\begin{aligned} in\Omega'_m r \left. \frac{\partial V}{\partial r} \right|_{r=r_m} &= \frac{\partial}{\partial \theta} \left( \sum_{m'} \tau_{m'}^{-1} \frac{\partial}{\partial \theta} \mathcal{J}_{m'} e^{i[m' \nu_m(\theta) - n\phi]} \right) \\ &= \frac{\partial}{\partial \theta} \left( \sum_{m'} \frac{im' \rho_m \mathcal{J}_{m'}}{\tau_{m'}} e^{i[m' \nu_m(\theta) - n\phi]} \right), \end{aligned} \quad (93)$$

where  $\Omega'_m = \Omega_m - \omega/n$  and  $\Omega_m$  is the plasma toroidal angular velocity at the surface. In addition, and for the sake of simplicity, let

$$\tau_m(\theta) = \rho_m \hat{\tau}_m, \quad (94)$$

$$\tau_{m' \neq m}(\theta) = \rho_m \zeta \hat{\tau}_m, \quad (95)$$

where  $\hat{\tau}_m$  and  $\zeta \ll 1$  are positive constants. Here,  $\hat{\tau}_m$  is the mean time-constant of the surface when responding to the resonant harmonic of the external perturbation and  $\zeta \hat{\tau}_m$  the much smaller mean time-constant when responding to non-resonant harmonics. This choice of time-constants ensures that the  $m, n$  resonant surface effectively only responds to the resonant harmonic of the perturbed magnetic field [i.e., the component of  $V(r_m, \theta, \phi)$  which varies as  $\exp(i[mv_m(\theta) - n\phi])$ ] and, furthermore, that the radially localized helical current excited at the surface flows predominately *parallel* to the local equilibrium magnetic field [i.e., the current stream-function varies as  $\exp(i[mv_m(\theta) - n\phi])$ ].

It follows from Eqs. (90)–(95) that

$$[V_{m'}]_{r_{m-}^{m+}} = \mathcal{J}_m U_{m'm}, \quad (96)$$

$$in\Omega_m' \hat{\tau}_m \sum_{m'} U_{m'm} r \frac{dV_{m'}}{dr} \Big|_{r_{m-}} = -m^2 \mathcal{J}_m, \quad (97)$$

where

$$U_{m'm} = \frac{1}{\pi} \int_0^\pi \cos[mv_m(\theta) - m'\theta] d\theta. \quad (98)$$

Furthermore,  $\mathcal{J}_{m \neq m'} \ll \mathcal{J}_m$ . Hence, from Eqs. (81), (96), and (97), the matching conditions at the simulated  $m, n$  resonant surface are

$$\left[ r \frac{dV_{m'}}{dr} \right]_{r_{m-}^{m+}} = 0, \quad (99)$$

$$[V_{m'}]_{r_{m-}^{m+}} = -i \frac{\Omega_m' \hat{\tau}_m}{n} \sum_{m''} \frac{U_{m'm} U_{m''m}}{q_m^2} r \frac{dV_{m''}}{dr} \Big|_{r_m}. \quad (100)$$

Now, the poloidal mode numbers of the various resonant surfaces lying within the plasma run from  $m_0$  to  $m_1$ , where

$$\frac{m_0 - 1}{n} < q_0 < \frac{m_0}{n} < \frac{m_1}{n} < q_p < \frac{m_1 + 1}{n}. \quad (101)$$

Here,  $q_0$  is the simulated central safety-factor of the plasma. For the sake of simplicity, let  $r_m \rightarrow 1_+$ ,  $h_m \rightarrow h_p$ ,  $\hat{\tau}_m \rightarrow \tau_p$ , and  $\Omega_m \rightarrow \Omega_p$  for all  $m_0 \leq m \leq m_1$ : i.e., let all of the rational surfaces lie just outside the plasma boundary, have the *same* mean time-constant  $\tau_p$  and rotate at the same toroidal angular velocity  $\Omega_p$ . In the following,  $\tau_p$  is interpreted as the mean time-scale for plasma dissipation and  $\Omega_p$  as the mean plasma toroidal angular velocity.

It follows, from the above, that the nonideal resonant response of the plasma can be incorporated into our analysis by replacing Eqs. (25)–(27) with

$$V_m(1_+) = -|m|^{-1} r \frac{dV_m}{dr} \Big|_{1_+} + i \frac{\Omega_p' \tau_p}{n} \times \sum_{m_0 \leq k \leq m_1, m'} \frac{U_{mk} U_{m'k}}{q_k^2} r \frac{dV_{m'}}{dr} \Big|_{1_+} + 2|m|^{-1} \Phi_m \quad (102)$$

for  $m \neq 0$ ,

$$V_0(1_+) = i \frac{\Omega_p' \tau_p}{n} \sum_{m_0 \leq k \leq m_1, m'} \frac{U_{0k} U_{m'k}}{q_k^2} r \frac{dV_{m'}}{dr} \Big|_{1_+} + b_0, \quad (103)$$

and

$$r \frac{dV_0}{dr} \Big|_{1_+} = a_0, \quad (104)$$

respectively. Here,  $\Omega_p' = \Omega_p - \omega/n$ .

## E. Matching at plasma boundary

The appropriate linearized matching conditions at  $r=1$  are<sup>18,19</sup>

$$\mathbf{e}_r \cdot \delta \mathbf{B}(r=1_-) = [\mathbf{B} \cdot \nabla \xi - \xi \mathbf{e}_r \cdot (\mathbf{e}_r \cdot \nabla) \mathbf{B}]_{r=1_-}, \quad (105)$$

$$\mathbf{e}_r \cdot \delta \mathbf{B}(r=1_+) = [\mathbf{B} \cdot \nabla \xi - \xi \mathbf{e}_r \cdot (\mathbf{e}_r \cdot \nabla) \mathbf{B}]_{r=1_+}, \quad (106)$$

$$[\mathbf{B} \cdot \delta \mathbf{B} + \xi \mathbf{e}_r \cdot \nabla(B^2/2)]_{r=1_-} = [\mathbf{B} \cdot \delta \mathbf{B} + \xi \mathbf{e}_r \cdot \nabla(B^2/2)]_{r=1_+}, \quad (107)$$

where  $\xi(\theta, \phi)$  is the normal plasma displacement at the boundary.

Let

$$\xi(\theta, \phi) = \sum_m \xi_m e^{i(m\theta - n\phi)}, \quad (108)$$

where the  $\xi_m$  are constants. The first matching condition yields

$$r \frac{dV_m}{dr} \Big|_{1_-} = \sum_{m'} E_{mm'} \xi_{m'}, \quad (109)$$

where

$$E_{mm'} = \frac{1}{\pi} \int_0^\pi (-nh_p) \cos[(m - m')\theta] d\theta. \quad (110)$$

The second matching condition gives

$$r \frac{dV_m}{dr} \Big|_{1_+} = \sum_{m'} G_{mm'} \xi_{m'}, \quad (111)$$

where

$$G_{mm'} = \frac{1}{\pi} \int_0^\pi (mB_p - nh_p) \cos[(m - m')\theta] d\theta. \quad (112)$$

Finally, the third matching condition reduces to

$$\sum_{m'} [E_{m'm} V_{m'}(1_-) - G_{m'm} V_{m'}(1_+)] = \sum_{m'} H_{mm'} \xi_{m'}, \quad (113)$$

where

$$H_{mm'} = \frac{1}{\pi} \int_0^\pi \left( \frac{B_p^2 h_p'}{h_p^2} + \beta x_p' \right) \cos[(m - m')\theta] d\theta, \quad (114)$$

$$h_p'(\theta) \equiv \frac{1}{2} \left. \frac{\partial([rh]^2)}{\partial r} \right|_{r=1} = (1 - E_p)^{-2} (1 - E_p^2 - 8T_p^2 + 6E_p T_p \cos \theta + 2T_p \cos 3\theta), \quad (115)$$

$$x_p'(\theta) \equiv r \left. \frac{\partial x}{\partial r} \right|_{r=1} = (1 - E_p)^{-1} [(1 + E_p) \cos \theta - 2T_p \cos 2\theta]. \quad (116)$$

**F. Plasma response equation**

Now, Eqs. (72) and (110) yield

$$\sum_{m'} E_{0m'} \xi_{m'} = 0. \quad (117)$$

But, as is clear from an examination of Eqs. (104) and (110)–(112), this implies that

$$\sum_{m'} G_{0m'} \xi_{m'} = r \left. \frac{dV_0}{dr} \right|_{1_+} = a_0 = 0. \quad (118)$$

Moreover, Eqs. (70), (71), and (109) give

$$V_m(1_-) = \sum_{k,m'} C_{mk} E_{km'} \xi_{m'} \quad (119)$$

for  $m \neq 0$  and

$$V_0(1_-) = \sum_{k,m'} C_{0k} E_{km'} \xi_{m'} + c_0. \quad (120)$$

Finally, Eqs. (102), (103), and (111) reduce to

$$V_m(1_+) = - \sum_{m'} |m|^{-1} G_{mm'} \xi_{m'} + i \frac{\Omega_p' \tau_p}{n} \times \sum_{m_0 \leq k \leq m_1, l, m'} \frac{U_{mk} U_{lk}}{q_k^2} G_{lm'} \xi_{m'} + 2|m|^{-1} \Phi_m \quad (121)$$

for  $m \neq 0$  and

$$V_0(1_+) = i \frac{\Omega_p' \tau_p}{n} \sum_{m_0 \leq k \leq m_1, l, m'} \frac{U_{0k} U_{lk}}{q_k^2} G_{lm'} \xi_{m'} + b_0. \quad (122)$$

Equation (113) can be combined with Eqs. (119)–(122) to give the *plasma response equation*,

$$\sum_{m'} F_{mm'} \xi_{m'} - i \frac{\Omega_p' \tau_p}{n} \sum_{k,m'} W_{mk} W_{m'k} \xi_{m'} = \sum_{k \neq 0} 2|k|^{-1} G_{km} \Phi_k + E_{0m} \Phi_0, \quad (123)$$

where

$$F_{mm'} = \sum_{k,l} E_{km} C_{kl} E_{lm'} + \sum_{k \neq 0} G_{km} |k|^{-1} G_{km'} - H_{mm'}, \quad (124)$$

$$W_{mm'} = \begin{cases} \sum_k U_{km'} G_{km} / q_m & m_0 \leq m' \leq m_1 \\ 0 & \text{otherwise,} \end{cases} \quad (125)$$

$$\Phi_0 = b_0 - c_0. \quad (126)$$

**G. Toroidal locking torque**

As is well-known, an external magnetic perturbation exerts a radially localized toroidal electromagnetic torque at each of the resonant surfaces lying within the plasma.<sup>12</sup> The torque exerted on the  $m, n$  surface (normalized to  $a^2 R_0 B_0^2 / \mu_0$ ) is

$$T_m = 2\pi^2 n \operatorname{Im} \left( \sum_{m'} r \left. \frac{dV_{m'}}{dr} \right|_{r_m} [V_{m'}]_{r_{m-}}^{r_{m+}} \right). \quad (127)$$

Thus, we deduce from Eq. (100) that

$$T_m = -2\pi^2 \Omega_m' \hat{\tau}_m \left( \sum_{m', m''} r \frac{dV_{m'}}{dr} \frac{U_{m'm} U_{m''m}}{q_m^2} r \frac{dV_{m''}}{dr} \right)_{r_m}. \quad (128)$$

Summing over all resonant surfaces, and taking the limit  $r_m \rightarrow 1_+$ ,  $\Omega_m \rightarrow \Omega_p$ ,  $\hat{\tau}_m \rightarrow \tau_p$ , we obtain the following expression for the total toroidal locking torque exerted on the plasma:

$$T_\phi = -2\pi^2 \Omega_p' \tau_p \left( \sum_{m, m_0 \leq k \leq m_1, m'} r \frac{dV_m^*}{dr} \frac{U_{mk} U_{m'k}}{q_k^2} r \frac{dV_{m'}}{dr} \right)_{1_+}. \quad (129)$$

Finally, making use of Eqs. (111) and (125), the above expression reduces to

$$T_\phi = -2\pi^2 \Omega_p' \tau_p \sum_{m, m'} \xi_m^* W_{mk} W_{m'k} \xi_{m'}. \quad (130)$$

**IV. INTRINSIC PLASMA STABILITY**

The intrinsic stability of the plasma to an ideal external-kink mode of toroidal mode number  $n$  is determined by solving plasma response equation (123) with  $\Omega_p'$ ,  $b_0$ , and all of the  $\Phi_m$ , set to zero (except  $\Phi_0 = -c_0$ ). This is equivalent to searching for a marginally stable ideal-MHD mode of toroidal mode number  $n$ , which corotates with the plasma (i.e.,  $\omega = n\Omega_p$ ), in the absence of an externally generated magnetic perturbation. The plasma response equation simplifies to

$$\vec{F}\vec{\xi} = \alpha_e \vec{e}, \quad (131)$$

where  $\vec{F}$  is the matrix of the  $F_{mm'}$  values,  $\vec{\xi}$  the column vector of the  $\xi_m$  values,  $\vec{e}$  the column vector of the

$$e_m = \frac{E_{0m}}{(\sum_{m'} E_{0m'} E_{0m'})^{1/2}} \quad (132)$$

values, and  $\alpha_e = \Phi_0 / (\sum_{m'} E_{0m'} E_{0m'})^{1/2}$ . Equation (131) must be solved subject to constraint (117), which implies that the poloidal cross-sectional area of the plasma is *invariant*, and which can be written as

$$\vec{e}^\dagger \vec{\xi} = 0, \quad (133)$$

where  $\vec{e}^\dagger$  is the row vector of the  $e_m^*$  values (i.e.,  $\dagger$  denotes a Hermitian conjugate). Note that  $\vec{e}^\dagger \vec{e} = 1$ .

Now, we can automatically satisfy the above constraint by writing<sup>18,19</sup>

$$\vec{\xi} = \vec{P}\vec{\xi}', \quad (134)$$

where

$$\vec{P} = \vec{I} - \vec{e}\vec{e}^\dagger. \quad (135)$$

Here,  $\vec{I}$  is the identity matrix. Note that  $\vec{e}^\dagger \vec{P} = \vec{P}\vec{e} = \vec{0}$ . Left-multiplying Eq. (131) by  $\vec{P}$ , we obtain

$$\vec{F}'\vec{\xi}' = 0, \quad (136)$$

where

$$\vec{F}' = \vec{P}\vec{F}\vec{P}. \quad (137)$$

Let the  $\vec{\xi}_j$  and  $\lambda_j$  be the eigenvectors and eigenvalues of the  $F'$ -matrix: i.e.,

$$\vec{F}'\vec{\xi}_j = \lambda_j \vec{\xi}_j. \quad (138)$$

Now, since  $F_{m'm} = F_{mm'}$ , which follows from Eqs. (75), (114), and (124), it is clear that the  $F'$ -matrix is Hermitian. Hence, the  $\lambda_j$  are real, and we can write

$$\vec{\xi}_i^\dagger \vec{\xi}_j = \delta_{ij}. \quad (139)$$

As is easily demonstrated, the  $F'$ -matrix possesses the trivial eigenvector  $\vec{\xi}_0 = \vec{e}$ , corresponding to the eigenvalue  $\lambda_0 = 0$ . However, from (134), this eigenvector generates a null plasma displacement and does not therefore correspond to a physical solution. Let  $\lambda_1$  be the most negative eigenvalue of the  $F'$ -matrix, excluding  $\lambda_0$ . According to the well-known *ideal-MHD energy principle*,<sup>9</sup> the plasma is intrinsically stable to an external-kink mode of toroidal mode number  $n$  (in the absence of a wall surrounding the plasma) when  $\lambda_1 > 0$  and is intrinsically unstable when  $\lambda_1 < 0$ . (This follows because  $\delta W = (1/2)\vec{\xi}'^\dagger \vec{F}' \vec{\xi}'$ , where  $\delta W$  is the ideal-MHD perturbed energy. Thus, if  $\vec{\xi}' = \vec{\xi}_j$  then  $\delta W = \lambda_j/2$ .) Hence, we deduce that the *no-wall stability limit* corresponds to  $\lambda_1 = 0$ .

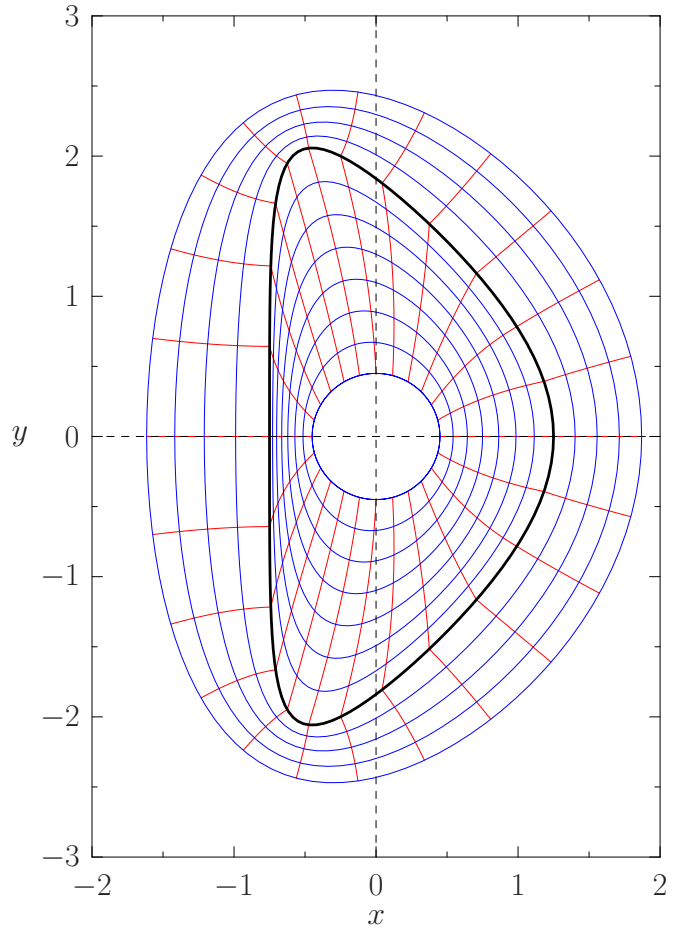


FIG. 1. (Color online) Poloidal cross-section of the equilibrium used in the example calculations. The equilibrium parameters are  $\kappa=2.0$ ,  $\delta=0.25$ , and  $r_0=0.3$ . The concentric (blue) curves show equally spaced (in  $r$ ) constant  $r$  surfaces. The radial (red) curves show equally spaced (in  $\theta$ ) constant  $\theta$  surfaces. The heavy (black) curve shows the plasma boundary.

## V. LOCKING TORQUE

The response of the plasma to a static (i.e.,  $\omega=0$ ), non-axisymmetric, externally generated, magnetic perturbation of toroidal mode number  $n$ —otherwise known as an error-field—is determined from plasma response equation (123), which can be written as

$$\vec{\xi}^\dagger \vec{\mathcal{F}} = \vec{\Phi}^\dagger \vec{M} + \alpha_e^* \vec{e}^\dagger, \quad (140)$$

where  $\vec{\mathcal{F}}$  is the matrix of the

$$\mathcal{F}_{mm'} = F_{mm'} + i \frac{\Omega_p \tau_p}{n} \sum_k W_{mk} W_{m'k} \quad (141)$$

values,  $\vec{\Phi}$  the column vector of the  $\Phi_m$  values, and  $\vec{M}$  the matrix of the

$$M_{mm'} = \begin{cases} 2|m|^{-1} G_{mm'} & m \neq 0 \\ 0 & m = 0 \end{cases} \quad (142)$$

values. The plasma response equation must again be solved subject to constraint (117), which can be written as

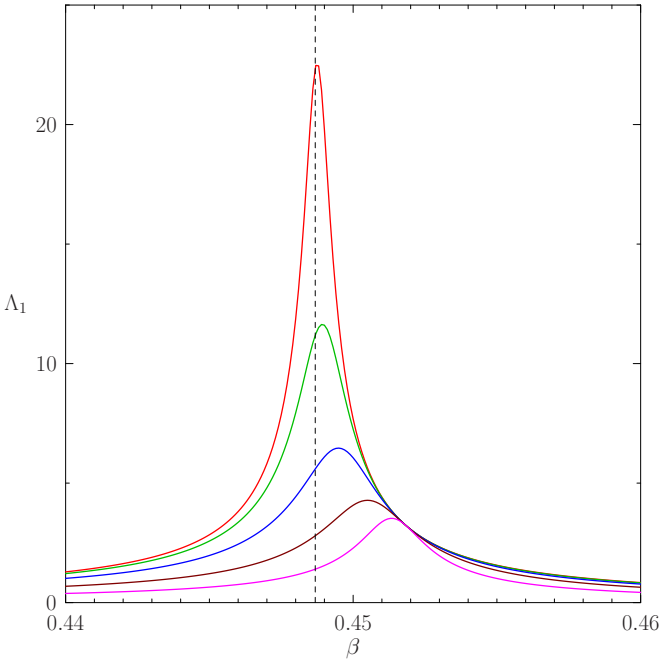


FIG. 2. (Color online) Singular value,  $\Lambda_1$ , associated with the  $j=1$  error-field, evaluated as a function of  $\beta$ . The first (red), second (green), third (blue), fourth (brown), and fifth (magenta) curves, in order from the top, correspond to  $\Omega_p \tau_p = 2.5, 5., 10., 20.,$  and  $40.$ , respectively. The other calculation parameters are  $\kappa=2.0, \delta=0.25, q_0=1.1, q_p=3.5, n=1, I=65,$  and  $r_0=0.3$ . The vertical dashed line indicates the no-wall stability limit.

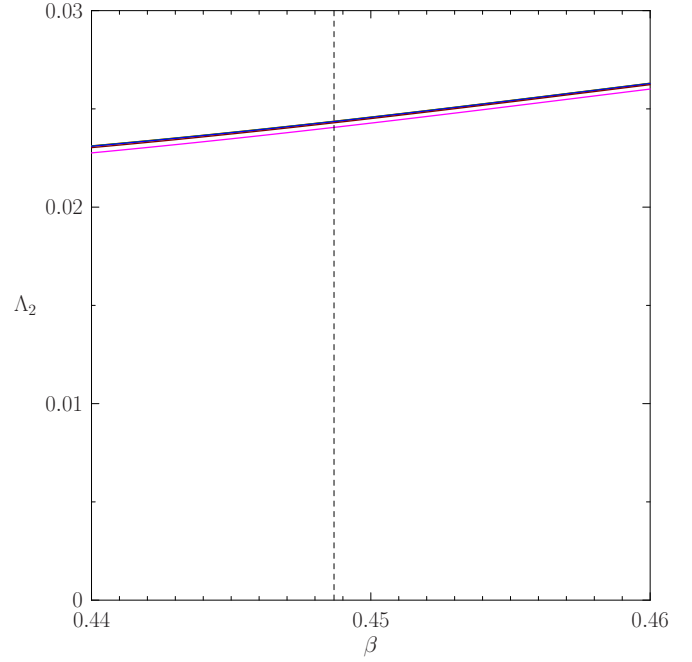


FIG. 3. (Color online) Singular value,  $\Lambda_2$ , associated with the  $j=2$  error-field, evaluated as a function of  $\beta$ . The various curves (which effectively plot on top of one another) correspond to  $\Omega_p \tau_p = 2.5, 5., 10., 20.,$  and  $40.$  The other calculation parameters are  $\kappa=2.0, \delta=0.25, q_0=1.1, q_p=3.5, n=1, I=65,$  and  $r_0=0.3$ . The vertical dashed line indicates the no-wall stability limit.

$$\xi^\dagger \vec{e} = 0. \tag{143}$$

Finally, from Eq. (130), the total toroidal electromagnetic torque exerted on the plasma by the error-field is

$$T_\phi = -2\pi^2 \Omega_p \tau_p |\xi^\dagger \vec{W}|^2, \tag{144}$$

where  $\vec{W}$  is the matrix of the  $W_{mm'}$  values.

Equations (140) and (143) can be combined to give

$$\xi^\dagger = \vec{\Phi}^\dagger \vec{M} \vec{L}, \tag{145}$$

where

$$\vec{L} = \vec{F}^{-1} - \vec{F}^{-1} \vec{e} \vec{e}^\dagger \vec{F}^{-1} / (\vec{e}^\dagger \vec{F}^{-1} \vec{e}). \tag{146}$$

Hence, Eq. (144) yields

$$T_\phi = -2\pi^2 \Omega_p \tau_p |\vec{\Phi}^\dagger \vec{X}|^2, \tag{147}$$

where

$$\vec{X} = \vec{M} \vec{L} \vec{W}. \tag{148}$$

Now,  $\vec{X}$ , which is referred to as the *plasma response matrix*, is a rectangular matrix of dimension  $I \times J$ , where  $I$  is the number of poloidal harmonics retained in the calculation and  $J$  the number of resonant surfaces lying within the plasma. It follows that  $I \geq J$ . According to a well-known theorem in linear algebra,<sup>26</sup> a matrix such as  $\vec{X}$  can always be decomposed as follows:

$$\vec{X} = \vec{Y} \vec{\Lambda} \vec{Z}, \tag{149}$$

where  $\vec{Y}$  is an  $I \times I$  matrix,  $\vec{\Lambda}$  an  $I \times J$  diagonal matrix, and  $\vec{Z}$  a  $J \times J$  matrix. Moreover,

$$\vec{Y} = \vec{y}_1 \vec{y}_2 \cdots \vec{y}_I, \tag{150}$$

where the  $\vec{y}_i$  are a complete set of orthonormal row vectors of length  $I$ : i.e.,

$$\vec{y}_i^\dagger \vec{y}_j = \delta_{ij} \tag{151}$$

for  $i, j=0, I$ . Likewise,

$$\vec{Z} = \vec{z}_1 \vec{z}_2 \cdots \vec{z}_J, \tag{152}$$

where the  $\vec{z}_i$  are a complete set of orthonormal row vectors of length  $J$ : i.e.,

$$\vec{z}_i^\dagger \vec{z}_j = \delta_{ij} \tag{153}$$

for  $i, j=0, J$ . Finally, the diagonal elements of  $\vec{\Lambda}$ , the  $\Lambda_i$  (say), are all *real* and *non-negative* and are arranged, such that  $\Lambda_1 > \Lambda_2 > \cdots > \Lambda_J$ . The type of decomposition described above is known as *singular value decomposition* and the  $\Lambda_i$  are called the *singular values*. For  $i=0, J$ , each  $\vec{y}_i$  and  $\vec{z}_i$  vector is associated with a corresponding nonzero singular value,  $\Lambda_i$ . On the other hand, for  $i=J+1, I$ , each  $\vec{y}_i$  vector is associated with the singular value of 0.

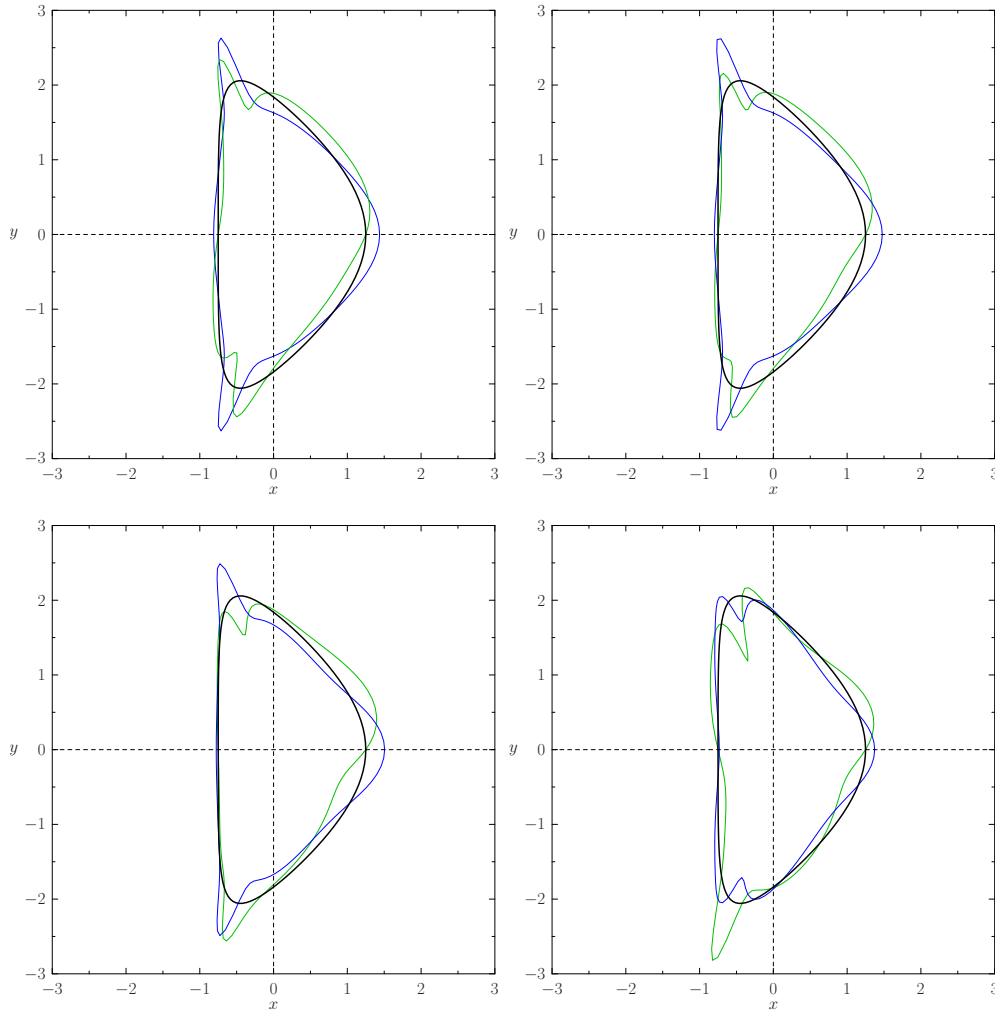


FIG. 4. (Color online) Independent components of the  $j=1$  normal error-field,  $C_1(\theta)$  (up-down symmetric, blue) and  $S_1(\theta)$  (up-down antisymmetric, green), plotted relative to the plasma boundary (heavy, black), for  $\beta=0.35$  (top left),  $0.40$  (top right),  $0.45$  (bottom left), and  $0.50$  (bottom right). The other calculation parameters are  $\kappa=2.0$ ,  $\delta=0.25$ ,  $q_0=1.1$ ,  $q_p=3.5$ ,  $\Omega_p\tau_p=10^{-3}$ ,  $n=1$ ,  $I=65$ , and  $r_0=0.3$ .

Let

$$\frac{\vec{\Phi}}{|\vec{\Phi}|} = \sum_{i=1, I} p_i \vec{y}_i. \tag{154}$$

It follows from Eq. (151) that

$$\sum_{i=1, I} |p_i|^2 = 1. \tag{155}$$

Furthermore, it is easily seen that

$$\vec{\Phi}^+ \vec{X} = \sum_{i=1, J} p_i^* \Lambda_i \vec{z}_i. \tag{156}$$

Thus, Eqs. (144) and (153) yield

$$T_\phi = -2\pi^2 \Omega_p \tau_p |\vec{\Phi}|^2 \sum_{i=1, J} |p_i|^2 \Lambda_i^2. \tag{157}$$

The  $J$  characteristic error-fields that are capable of exerting a torque on the plasma are such that

$$\frac{\vec{\Phi}_j}{|\vec{\Phi}_j|} = \vec{y}_j \tag{158}$$

for  $j=1, J$ . The corresponding torques are<sup>15</sup>

$$T_j = -2\pi^2 \Omega_p \tau_p \Lambda_j^2 |\vec{\Phi}_j|^2. \tag{159}$$

On the other hand, the  $I-J$  independent error-fields that exert zero torque on the plasma are such that

$$\frac{\vec{\Phi}_j}{|\vec{\Phi}_j|} = \vec{y}_j \tag{160}$$

for  $j=J+1, I$ . Now, according to Eqs. (30) and (31), the poloidal variation of the normal component of the  $j$ th independent error-field (in vacuum) at a given toroidal location on the plasma boundary is a linear combination of  $C_j(\theta)$  and  $S_j(\theta)$ , where

$$C_j(\theta) = \frac{1}{h_p(\theta)} \sum_{m \neq 0} [\text{Re}(\vec{y}_j)_m \cos(m\theta) - \text{Im}(\vec{y}_j)_m \sin(m\theta)], \tag{161}$$

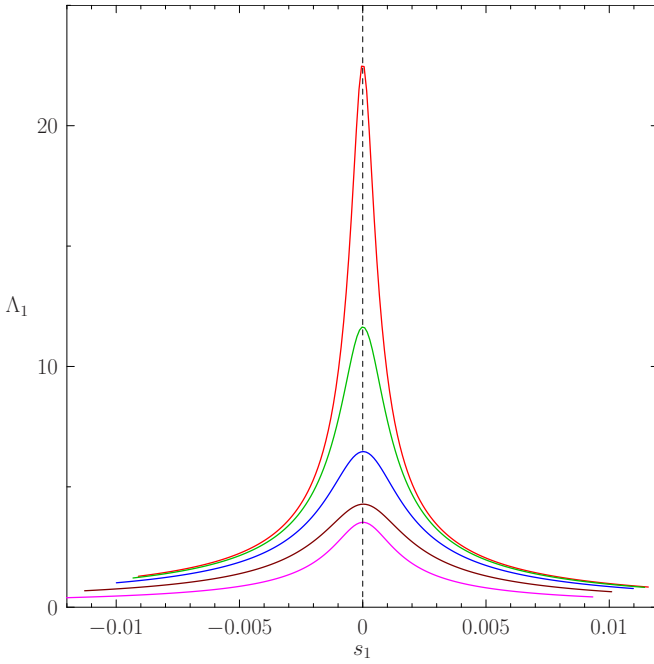


FIG. 5. (Color online) Singular value,  $\Lambda_1$ , associated with the  $j=1$  error-field, evaluated as a function of the related Boozer parameter,  $s_1$ . The first (red), second (green), third (blue), fourth (brown), and fifth (magenta) curves, in order from the top, correspond to  $\Omega_p \tau_p = 2.5, 5, 10, 20,$  and  $40,$  respectively. The other calculation parameters are  $\kappa=2.0, \delta=0.25, q_0=1.1, q_p=3.5, n=1, I=65,$  and  $r_0=0.3$ .

$$S_j(\theta) = \frac{1}{h_p(\theta)} \sum_{m \neq 0} [\text{Re}(\vec{y}_j)_m \sin(m\theta) + \text{Im}(\vec{y}_j)_m \cos(m\theta)]. \quad (162)$$

Finally, a comparison of Eqs. (155) and (157) reveals that the  $j=1$  error-field *maximizes* the total toroidal electromagnetic torque exerted on the plasma, at fixed  $|\vec{\Phi}|$ .<sup>15</sup> Of course, if the  $j=1$  error-field is excluded then the  $j=2$  error-field maximizes the torque, and so on.

## VI. BOOZER PARAMETERS

Equations (35), (111), (130), and (140)–(143) yield<sup>27</sup>

$$2\delta W + i \frac{\tau_\phi}{n} = \vec{\chi}^\dagger \vec{N} \vec{\Phi}, \quad (163)$$

where  $\delta W = (1/2) \vec{\xi}^\dagger \vec{F} \vec{\xi}$  is the ideal-MHD perturbed energy,  $\tau_\phi = T_\phi / 2\pi^2$ ,  $\vec{\chi}$  is the column vector of the  $\chi_m$  values, and  $\vec{N}$  the matrix of the

$$N_{mm'} = \begin{cases} 2|m|^{-1} \delta_{mm'} & m \neq 0 \\ 0 & m = 0 \end{cases} \quad (164)$$

values. Now, it is conventional to write<sup>28</sup>

$$-\frac{\vec{\chi}^\dagger \vec{N} \vec{\Phi}}{\vec{\chi}^\dagger \vec{N} \vec{\chi}} = s_B + i\alpha_B, \quad (165)$$

where the so-called *Boozer parameters*  $s_B$  and  $\alpha_B$  are both real. These particular dimensionless parameters are significant because they can be measured experimentally.<sup>29</sup>

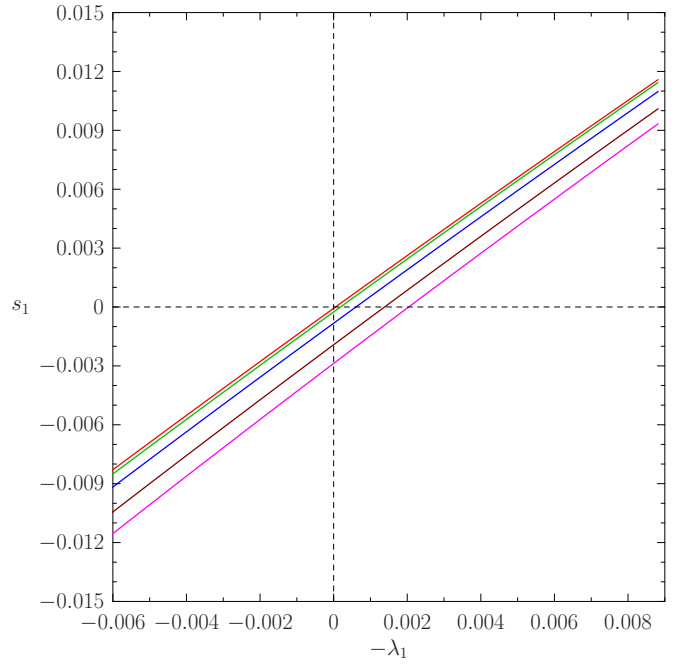


FIG. 6. (Color online) Boozer parameter,  $s_1$ , associated with the  $j=1$  error-field, evaluated as a function of the plasma stability parameter,  $\lambda_1$ . The first (red), second (green), third (blue), fourth (brown), and fifth (magenta) curves, in order from the top, correspond to  $\Omega_p \tau_p = 2.5, 5, 10, 20,$  and  $40,$  respectively. The other calculation parameters are  $\kappa=2.0, \delta=0.25, q_0=1.1, q_p=3.5, n=1, I=65,$  and  $r_0=0.3$ .

Moreover, the Boozer parameters associated with the  $j$ th characteristic error-field, obtained via singular value decomposition of the plasma response matrix (see Sec. V), are

$$s_j + i\alpha_j \equiv - \left( \frac{\vec{x}_j^\dagger \vec{N} \vec{y}_j}{\vec{x}_j^\dagger \vec{N} \vec{x}_j} \right) = - \left( \frac{\vec{\xi}_j^\dagger \vec{F} \vec{\xi}_j}{\vec{x}_j^\dagger \vec{N} \vec{x}_j} \right) + i \frac{\Omega_p \tau_p}{n} \left( \frac{\Lambda_j^2}{\vec{x}_j^\dagger \vec{N} \vec{x}_j} \right), \quad (166)$$

where  $\vec{x}_j = \vec{G} \vec{\xi}_j$  and  $\vec{\xi}_j = \vec{L}^\dagger \vec{M}^\dagger \vec{y}_j$ .

## VII. EXAMPLE CALCULATIONS

Consider the response of a strongly shaped tokamak plasma of vertical elongation  $\kappa=2.0$ , triangularity  $\delta=0.25$ , and central safety-factor  $q_0=1.1$ , to an  $n=1$  error-field. The plasma boundary and the associated  $r-\theta$  coordinate surfaces (for  $r_0=0.3$ ) are shown in Fig. 1. All of the calculations discussed below employ 65 poloidal harmonics, ranging from  $m=-32$  to  $+32$ , and are such that internal solutions are launched from  $r_0=0.3$ .

Figures 2 and 3 show the two nonzero singular values of the error-field response matrix,  $\Lambda_1$  and  $\Lambda_2$ , calculated as functions of  $\beta$ , for  $q_p=3.5$ , and various different values of the normalized plasma rotation,  $\Omega_p \tau_p$ . Also shown is the  $n=1$  no-wall beta-limit, which lies at  $\beta_{nw}=0.4487$ . (So, in the absence of a wall, the plasma is stable to the  $n=1$  external-kink mode when  $\beta < \beta_{nw}$  and unstable when  $\beta > \beta_{nw}$ .) Incidentally, there are only two nonzero singular values because there are only two resonant surfaces lying within the plasma (namely, the  $q=2$  and  $q=3$  surfaces).

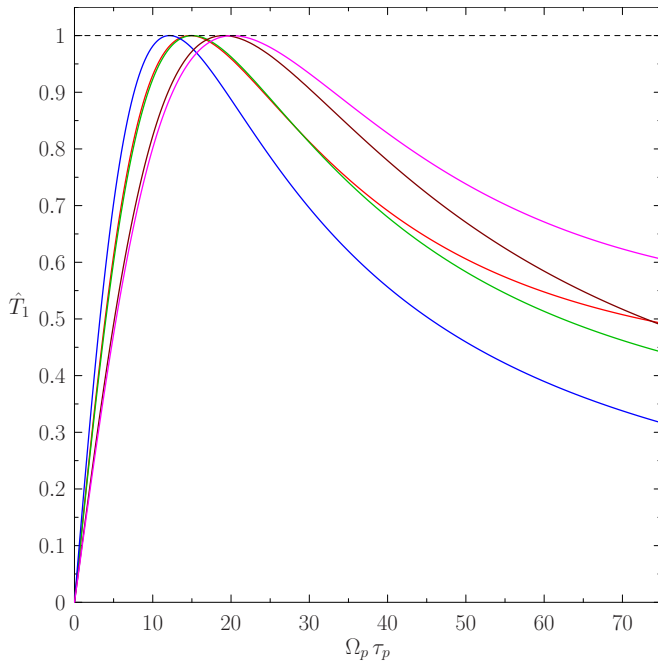


FIG. 7. (Color online) Normalized locking torque,  $\hat{T}_1$ , due to the  $j=1$  error-field, evaluated as a function of  $\Omega_p \tau_p$ . The second (red), third (green), first (blue), fourth (brown), and fifth (magenta) curves, in order from the left, correspond to  $\beta=0.35, 0.40, 0.45, 0.50$ , and  $0.55$ , respectively. The other calculation parameters are  $\kappa=2.0, \delta=0.25, q_0=1.1, q_p=3.5, n=1, I=65$ , and  $r_0=0.3$ .

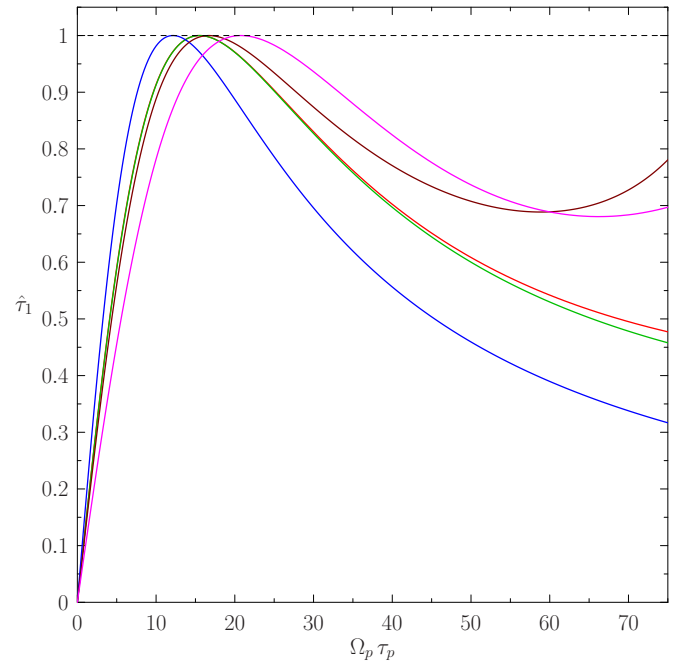


FIG. 9. (Color online) Normalized Boozer locking torque,  $\hat{\tau}_1$ , due to the  $j=1$  error-field, evaluated as a function of  $\Omega_p \tau_p$ . The third (red), second (green), first (blue), fourth (brown), and fifth (magenta) curves, in order from the left, correspond to  $\beta=0.35, 0.40, 0.45, 0.50$ , and  $0.55$ , respectively. The other calculation parameters are  $\kappa=2.0, \delta=0.25, q_0=1.1, q_p=3.5, n=1, I=65$ , and  $r_0=0.3$ .

A comparison of Figs. 2 and 3 reveals that  $\Lambda_1 \gg \Lambda_2$ . Since, at fixed plasma rotation and error-field amplitude, the locking torque associated with the  $j$ th independent error-field is proportional to  $\Lambda_j^2$  [see Eq. (159)], we conclude that the

torque exerted by the  $j=2$  error-field is completely negligible compared to that exerted by the  $j=1$  error-field. Moreover, these are the only two independent error-fields that are capable of exerting a torque on the plasma. It follows that, for the particular equilibrium under investigation, we can effectively eliminate the locking torque associated with a general error-field by simply canceling out the field's  $j=1$  component using correction coils.<sup>13-15</sup>

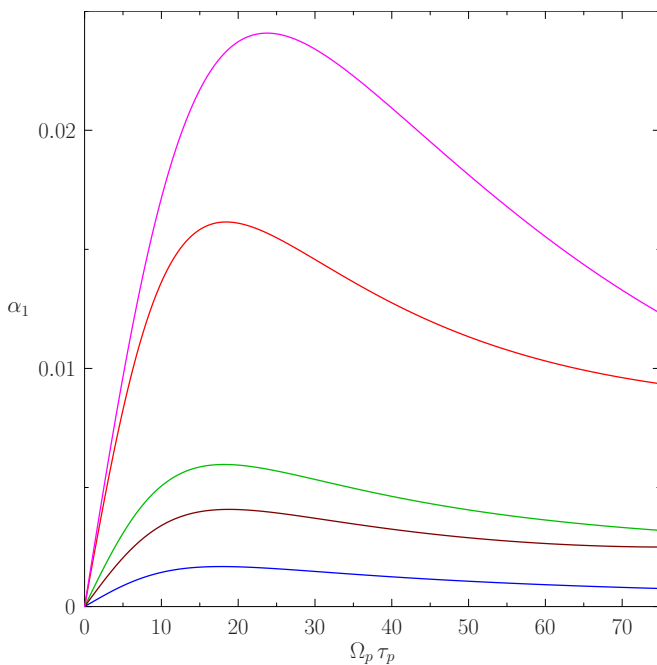


FIG. 8. (Color online) Boozer parameter  $\alpha_1$ , associated with the  $j=1$  error-field, evaluated as a function of  $\Omega_p \tau_p$ . The second (red), third (green), fifth (blue), fourth (brown), and first (magenta) curves, in order from the top, correspond to  $\beta=0.35, 0.40, 0.45, 0.50$ , and  $0.55$ , respectively. The other calculation parameters are  $\kappa=2.0, \delta=0.25, q_0=1.1, q_p=3.5, n=1, I=65$ , and  $r_0=0.3$ .

Figure 4 illustrates the poloidal variation of the normal component of the  $j=1$  error-field at the plasma boundary. This is calculated for various different values of  $\beta$ , at low plasma rotation (i.e.,  $\Omega_p \tau_p \ll 1$ ). Now, at a given toroidal location on the boundary, the variation in question is a linear combination of two functions,  $C_1(\theta)$  and  $S_1(\theta)$ , which are plotted in the figure (relative to the boundary). As can be seen, in the absence of strong plasma rotation (or strong dissipation), the first of these functions is up-down symmetric, and the second up-down antisymmetric. Observe that the  $C_1(\theta)$  and  $S_1(\theta)$  functions attain their peak amplitudes at the top and bottom of the plasma, where the boundary's radius of curvature becomes especially small, indicating a particularly sensitivity to external magnetic perturbations at these locations. Moreover, the functions have negligible amplitude on the inboard side of the plasma, indicating a total insensitive to inboard external magnetic perturbations.<sup>13-15</sup>

As is apparent from Fig. 2, the dominant singular value of the error-field response matrix,  $\Lambda_1$ , exhibits a resonant peak (as  $\beta$  varies) close to the no-wall beta-limit,  $\beta = \beta_{nw}$ . This implies that the locking torque associated with a general error-field also peaks strongly when  $\beta \approx \beta_{nw}$ . As is well-known, this peaking is due to a resonant amplification of the

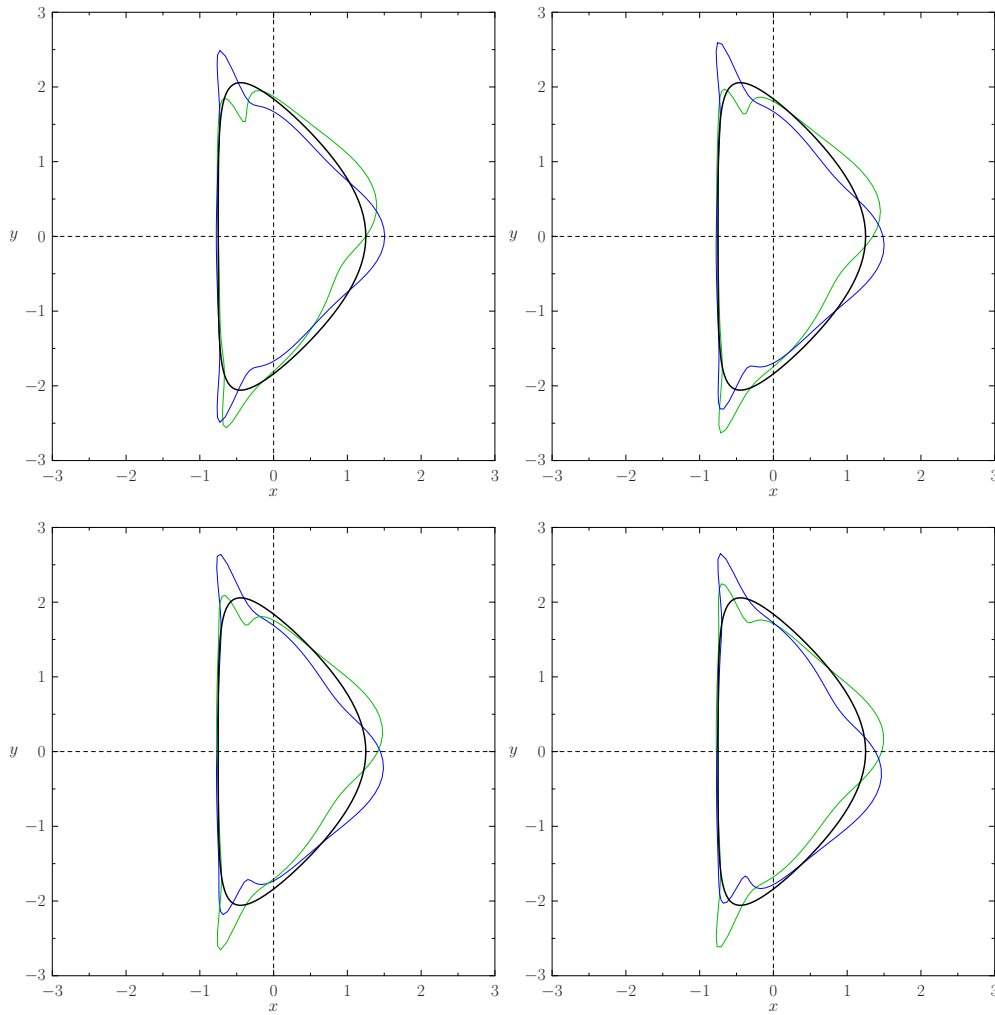


FIG. 10. (Color online) Independent components of the  $j=1$  normal error-field,  $C_1(\theta)$  (first from the top, blue) and  $S_1(\theta)$  (first from the bottom, green), plotted relative to the plasma boundary (heavy, black), for  $\Omega_p \tau_p = 10^{-3}$  (top left), 5. (top right), 10. (bottom left), and 20. (bottom right). The other calculation parameters are  $\kappa=2.0$ ,  $\delta=0.25$ ,  $\beta=0.45$ ,  $q_0=1.1$ ,  $q_p=3.5$ ,  $n=1$ ,  $I=65$ , and  $r_0=0.3$ .

$j=1$  error-field by the plasma.<sup>28</sup> Observe that the peak value of  $\Lambda_1$  is approximately inversely proportional to the normalized plasma rotation  $\Omega_p \tau_p$ .<sup>28</sup> Moreover, as the level of rotation increases, the resonance peak shifts to the high- $\beta$  side of the no-wall beta-limit. Such behavior indicates that, in the presence of substantial plasma rotation (or, alternatively, substantial plasma dissipation), the error-field torque peaks at a beta value that lie *above* the no-wall stability limit (i.e.,  $\beta > \beta_c$ ). This prediction is consistent with experimental observations.<sup>17,29,30</sup> Note, finally, from Fig. 3, that the second largest singular value of the error-field response matrix,  $\Lambda_2$ , does not exhibit any resonant behavior in the vicinity of the no-wall beta-limit.

Figure 5 shows the dominant singular value of the error-field response matrix,  $\Lambda_1$ , evaluated as a function of the associated Boozer parameter  $s_1$  for a range of beta values around the no-wall beta-limit and for various different values of the plasma rotation. It can be seen that, irrespective of the level of rotation, the peak value of  $\Lambda_1$  corresponds to  $s_1=0$ . It follows that the peak locking torque (at constant error-field amplitude and plasma rotation) also always occurs when  $s_1=0$ .<sup>28</sup>

Figure 6 illustrates the relationship between the Boozer parameter  $s_1$  associated with the  $j=1$  error-field and the plasma stability parameter  $\lambda_1$ . Recall, from Sec. IV, that the plasma is stable to the no-wall  $n=1$  external-kink mode when  $\lambda_1 > 0$  and unstable when  $\lambda_1 < 0$ . It can be seen that the no-wall beta-limit,  $\lambda_1=0$ , corresponds to  $s_1=0$  at low plasma rotation levels. However, at higher rotation levels, the Boozer parameter  $s_1$  passes through zero when  $\lambda_1 < 0$ : i.e., at beta values above the no-wall beta-limit. Thus, in general,  $s_1=0$ , which corresponds to the peak locking torque, *does not* correspond to the no-wall beta-limit,<sup>31</sup> as erroneously stated in Ref. 28.

Figure 7 shows the locking torque,

$$T_1 \propto \Omega_p \tau_p \Lambda_1^2, \quad (167)$$

associated with the dominant  $j=1$  error-field, calculated as a function of the normalized plasma rotation,  $\Omega_p \tau_p$ , and normalized such that its peak value is unity. The torque is evaluated for various different values of  $\beta$ . It can be seen that the torque initially increases linearly with increasing plasma rotation, but eventually attains a maximum value, and thereaf-

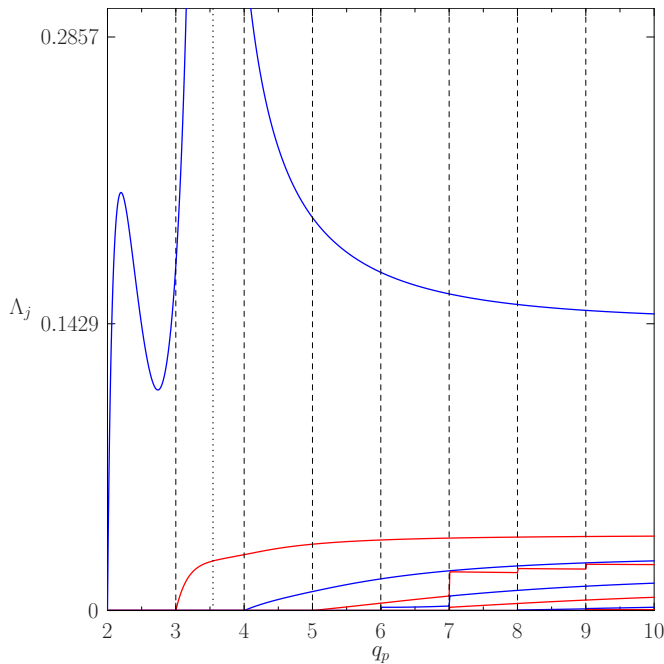


FIG. 11. (Color online) Nonzero singular values of the plasma response matrix, evaluated as a function of  $q_p$ . The other calculation parameters are  $\kappa=2.0$ ,  $\delta=0.25$ ,  $\beta=0.45$ ,  $q_0=1.1$ ,  $\Omega_p\tau_p=20$ ,  $n=1$ ,  $I=65$ , and  $r_0=0.3$ . The vertical dotted line indicates the no-wall stability limit.

ter decreases with increasing rotation. This variation of the torque is caused by decreasing plasma amplification of the  $j=1$  error-field with increasing plasma rotation.

Figure 8 illustrates the relationship between the Boozer parameter  $\alpha_1$  associated with the dominant  $j=1$  error-field, and the normalized plasma rotation,  $\Omega_p\tau_p$ . At low rotation levels, it can be seen that  $\alpha_1 \propto \Omega_p\tau_p$ . However, at higher rotation levels,  $\alpha_1$  attains a peak value and, thereafter, decreases with increasing plasma rotation.

Figure 9 shows the Boozer single-mode prediction for the locking torque associated with the dominant  $j=1$  error-field,<sup>28</sup>

$$\tau_1 \propto \frac{\alpha_1}{s_1^2 + \alpha_1^2}, \quad (168)$$

calculated as a function of the normalized plasma rotation,  $\Omega_p\tau_p$ , and normalized such that its peak value is unity. The torque is evaluated for various different values of  $\beta$ . It can be seen, by comparison with Fig. 7, that the Boozer prediction actually does a reasonably good job of accounting for the variation of the locking torque with plasma rotation at low to moderate levels of rotation.

Figure 10 shows the poloidal variation of the normal component of the  $j=1$  error-field at the plasma boundary, calculated for various different values of the normalized plasma rotation,  $\Omega_p\tau_p \ll 1$ , at a beta value close to the no-wall beta-limit. It can be seen that, in the presence of strong plasma rotation or strong dissipation (i.e.,  $\Omega_p\tau_p \gg 1$ ), the  $C_1(\theta)$  and  $S_1(\theta)$  functions deviate significantly from pure up-down symmetric and pure up-down antisymmetric functions, respectively.

Finally, Fig. 11 shows the nonzero singular values of the

plasma response matrix,  $\Lambda_j$ , calculated as a function of  $q_p$  for fixed  $q_0$ ,  $\beta$ , and  $\Omega_p\tau_p$ . Also shown is the no-wall stability limit, which corresponds to  $q_{pnw}=3.544$ . (So, in the absence of a wall, the plasma is stable to an  $n=1$  external-kink mode when  $q_p > q_{pnw}$  and unstable when  $q_p < q_{pnw}$ .) Note that the largest singular value  $\Lambda_1$  has a resonant peak when  $q_p \approx q_{pnw}$ . Now, as  $q_p$  increases at constant  $q_0$ , a new nonzero singular value appears each time a resonant surface enters the plasma from the boundary. Observe that these new values become progressively smaller. Moreover, each singular value asymptotes to a finite constant as  $q_p \rightarrow \infty$ . This suggests that, in the limit  $q_p \rightarrow \infty$ , in which there are an infinite number of resonant surfaces within the plasma, and a magnetic X-point appears on the boundary, the locking torque exerted by a general error-field remains *finite*. Finally, it can be seen that some of the singular values (e.g.,  $\Lambda_5$  and  $\Lambda_6$ ) are *nonzero* when they first appear. This implies that the locking torque due to a general error-field can increase *discontinuously* when a resonant surface enters the plasma from the boundary.<sup>32</sup>

## VIII. SUMMARY

A model has been developed in order to predict the error-field response of a toroidally rotating tokamak plasma possessing a strongly shaped poloidal cross-section. The response is made up of nondissipative ideal and dissipative nonideal components. The calculation of the ideal response is greatly simplified by employing a large aspect-ratio, constant pressure, plasma equilibrium in which the current is entirely concentrated at the boundary. Moreover, the calculation of the resonant component of the nonideal response is simplified by modeling each resonant surface within the plasma as a toroidally rotating, thin resistive shell that only responds to the resonant component of the perturbed magnetic field. This approach mimics dissipation due to continuum damping at Alfvén and/or sound wave resonances located close to each surface. The nonresonant component of the nonideal response is neglected. The error-fields that maximize the net toroidal electromagnetic torque exerted on the plasma are determined via singular value decomposition of the total response matrix.

For a strongly dissipative plasma, the toroidal locking torque associated with a general error-field is found to peak at a beta value that lies above the no-wall beta-limit, in accordance with experimental observations. In addition, the torque exhibits a nonmonotonic variation with increasing plasma rotation. The torque also asymptotes to a finite value as  $q_p \rightarrow \infty$ , indicating that it remains *finite* when there is a magnetic X-point on the boundary. Finally, the torque is able to increase discontinuously when a resonant surface enters the plasma from the boundary.

## ACKNOWLEDGMENTS

This research was funded by the U.S. Department of Energy.

<sup>1</sup>J. A. Wesson, *Tokamaks*, 3rd ed. (Oxford University Press, Oxford, 2004).

<sup>2</sup>J. T. Scoville, R. J. La Haye, A. G. Kellman, T. H. Osborne, R. D.

- Stambaugh, E. J. Strait, and T. S. Taylor, *Nucl. Fusion* **31**, 875 (1991).
- <sup>3</sup>T. C. Hender, R. Fitzpatrick, A. W. Morris, P. G. Carolan, R. D. Durst, T. Edlington, J. Ferreira, S. J. Fielding, P. S. Haynes, J. Hugill, I. J. Jenkins, R. J. La Haye, B. J. Parham, D. C. Robinson, T. N. Todd, M. Valovic, and G. Vayakis, *Nucl. Fusion* **32**, 2091 (1992).
- <sup>4</sup>G. M. Fishpool and P. S. Haynes, *Nucl. Fusion* **34**, 109 (1994).
- <sup>5</sup>R. J. Buttery, M. De Benedetti, T. C. Hender, and B. J. D. Tubbing, *Nucl. Fusion* **40**, 807 (2000).
- <sup>6</sup>S. M. Wolfe, I. H. Hutchinson, R. S. Granetz, J. Rice, A. Hubbard, A. Lynn, P. Phillips, T. C. Hender, and D. F. Howell, *Phys. Plasmas* **12**, 056110 (2005).
- <sup>7</sup>A. H. Boozer, *Rev. Mod. Phys.* **76**, 1071 (2005).
- <sup>8</sup>Z. Chang and J. D. Callen, *Nucl. Fusion* **30**, 219 (1990).
- <sup>9</sup>J. P. Freidberg, *Ideal Magnetohydrodynamics* (Springer, New York, 1987).
- <sup>10</sup>R. Fitzpatrick, *Nucl. Fusion* **33**, 1049 (1993).
- <sup>11</sup>R. Fitzpatrick, *Phys. Plasmas* **5**, 3325 (1998).
- <sup>12</sup>R. Fitzpatrick, R. J. Hastie, T. J. Martin, and C. M. Roach, *Nucl. Fusion* **33**, 1533 (1993).
- <sup>13</sup>J.-K. Park, A. H. Boozer, and A. H. Glasser, *Phys. Plasmas* **14**, 052110 (2007).
- <sup>14</sup>J.-K. Park, M. J. Schaffer, J. E. Menard, and A. H. Boozer, *Phys. Rev. Lett.* **99**, 195003 (2007).
- <sup>15</sup>J.-K. Park, A. H. Boozer, J. E. Menard, and M. J. Schaffer, *Nucl. Fusion* **48**, 045006 (2008).
- <sup>16</sup>A. H. Boozer, *Phys. Plasmas* **16**, 052505 (2009).
- <sup>17</sup>H. Reimerdes, A. M. Garofalo, E. J. Strait, R. J. Buttery, M. S. Chu, Y. In, G. L. Jackson, R. J. La Haye, M. J. Lanctot, Y. Q. Liu, M. Okabayashi, J.-K. Park, M. J. Schaffer, and W. M. Solomon, *Nucl. Fusion* **49**, 115001 (2009).
- <sup>18</sup>J. P. Freidberg and F. Haas, *Phys. Fluids* **16**, 1909 (1973).
- <sup>19</sup>J. P. Freidberg and F. Haas, *Phys. Fluids* **17**, 440 (1974).
- <sup>20</sup>J. P. Freidberg and W. Grossmann, *Phys. Fluids* **18**, 1494 (1975).
- <sup>21</sup>L. Chen and A. Hasegawa, *Phys. Fluids* **17**, 1399 (1974).
- <sup>22</sup>J. B. Taylor, *Phys. Rev. Lett.* **91**, 115002 (2003).
- <sup>23</sup>R. Fitzpatrick, *Phys. Plasmas* **1**, 3308 (1994).
- <sup>24</sup>A. Bondeson and D. J. Ward, *Phys. Rev. Lett.* **72**, 2709 (1994).
- <sup>25</sup>R. Betti and J. P. Freidberg, *Phys. Rev. Lett.* **74**, 2949 (1995).
- <sup>26</sup>G. H. Golub and C. F. Van Loan, *Matrix Computations*, 3rd ed. (Johns Hopkins, Baltimore, MD, 1996).
- <sup>27</sup>A. H. Boozer, *Phys. Plasmas* **10**, 1458 (2003).
- <sup>28</sup>A. H. Boozer, *Phys. Rev. Lett.* **86**, 5059 (2001).
- <sup>29</sup>J.-K. Park, A. H. Boozer, J. E. Menard, S. P. Gerhardt, and S. A. Sabbagh, *Phys. Plasmas* **16**, 082512 (2009).
- <sup>30</sup>M. J. Lanctot, H. Reimerdes, A. M. Garofalo, M. S. Chu, Y. Q. Liu, E. J. Strait, G. L. Jackson, R. J. La Haye, M. Okabayashi, T. H. Osbourne, and M. J. Schaffer, *Phys. Plasmas* **17**, 030701 (2010).
- <sup>31</sup>V. D. Pustovitov, *Plasma Phys. Rep.* **30**, 187 (2004).
- <sup>32</sup>R. Fitzpatrick and T. C. Hender, *Phys. Plasmas* **1**, 3337 (1994).